

SHEAR STRENGTH AND DEFORMATION CAPACITY OF INTERIOR R/C BEAM-COLUMN JOINT SUBASSEMBLAGE

HIDEO MURAKAMI¹, SHIGERU FUJII², YASUHIRO ISHIWATA³ And SHIRO MORITA⁴

SUMMARY

Collecting available 332 test data, the database of interior R/C beam-column joint subassembly was constructed. Analysing the specimens failed in joint shear without plastic hinge development at adjacent beams, the parameters affecting on joint shear strength were examined and the strength equation was proposed statistically. The deformation capacity of beam-column joint subassembly that failed in joint shear with inelastic deformations of adjacent beams was examined and the ductility ratio of subassembly governed by joint shear failure was formulated. These equations provide a good agreement between calculated and measured. The final failure modes of subassembly could be predicted with good accuracy.

INTRODUCTION

In Japan, seismic design requirement of interior R/C beam-column joint was firstly introduced in *Design Guideline for Earthquake Resistant Reinforced Concrete Building Based on Ultimate Strength Concept (1988)*. However, in recent years, many experimental data including the specimens with high strength materials were reported. And, it is acknowledged that evaluations of not only joint shear strength but also deformation capacity are essential to establish the performance-based-design method in R/C moment resisting frames. Based on the above standpoints, the statistical database analysis was conducted. The proposed equations in this paper were adopted into *Design Guideline for Earthquake Resistant Reinforced Concrete Building Based on Inelastic Displacement Concept (Draft) (1997)*.

DATABASE OF INTERIOR R/C BEAM-COLUMN JOINT

Experimental data of interior R/C beam-column joint subassembly subjected to seismic loading was collected from literatures published from 1976 to 1993. The total number of the collected data was 332. The database includes the information of bar arrangement, material strength, characteristic points of the envelope in beam shear force - story drift curves, and failure modes and so on.

Failure modes of the specimens were classified to three types: flexural failure of adjacent beams without significant shear deterioration in joint regions [F-type], joint shear failure after flexural yielding in adjacent beams [FS-type] and joint shear failure before flexural yielding in adjacent beams [S-type]. The numbers of the specimens of F-type, FS-type and S-type failure were 129, 144 and 59 respectively.

Range of experimental parameters is shown in Table 1. Concrete compressive strength [σ_B] was varied in 18MPa $\leq \sigma_B \leq 117$ MPa. Concrete strengths of nearly half specimens were less than 40MPa. Column axial force ratio [$\eta = N / (b_c \cdot D_c \cdot \sigma_B)$, where N : column axial force, b_c : column width and D_c : column depth] was varied in the range of

¹ Research Institute of Technology, Konoike Construction Co. Ltd. 1-20-1 Sakura, Tsukuba City, Ibaraki 305-0003, Japan

² Graduate School of Engineering, Kyoto University Yoshidahonmachi Sakyo-ku, Kyoto, 606-8501, Japan

³ Technical Research Institute, Tekken Corporation Co. Ltd. 9-1 Shin-Izumi, Narita City, Chiba 286-0825, Japan

⁴ General Building Research Corporation of Japan 5-8-1 Fujishirodai, Suita City, Osaka 565-0873, Japan

$0 \leq \eta \leq 0.485$, and three-quarters of all specimens have η of less than 0.2. The range of joint shear reinforcement ratio [p_w] was $0\% \leq p_w \leq 2.44\%$ and about 40% of all specimens were in the range of $0.2\% \leq p_w < 0.5\%$.

DEFINITION OF JOINT SHEAR STRESS

The specimen configuration and the loading condition are shown in Figure 1. The joint shear stress [τ_j] is defined by Equation (1), where the effective joint width [b_j] is an average of column width [b_c] and beam width [b_b].

$$\tau_j = \frac{Q_j}{b_j \cdot D_j} \quad \text{--- (1)}$$

$$Q_j = \frac{M_{b1}}{j_1} + \frac{M_{b2}}{j_2} - Q_c = (Q_{b1} + Q_{b2}) \cdot \left\{ \frac{L_o / 2}{j} - \frac{L_o + D_c}{2 \cdot (H_o + D_b)} \right\} \quad \text{--- (2)}$$

$$b_j = \frac{b_c + b_b}{2} \quad \text{--- (3)}$$

Where, τ_j : joint shear stress, Q_j : joint shear force, Q_c : column shear force, Q_b : beam shear force, M_b : beam moment, b_c : column width, b_b : beam width, D_c : column depth, D_b : beam depth, b_j : joint effective width, D_j : joint effective depth [= D_c], H_o : column clear span, L_o : beam clear span and j : internal lever arm at beam section [= $(7/8) \cdot d$, d : beam effective depth].

SHEAR STRENGTH OF ELASTIC JOINTS

Joint shear strength was examined analysing the 50 S-type specimens without transverse beams. As shown in Figure 2, the regression analysis indicates that the joint shear strength [${}_c\tau_p$] for the specimens failed in shear before beam yielding is proportional to the function of concrete compressive strength, $\sigma_B^{0.712}$. It can be formulated by the Equation (4).

$${}_c\tau_p = 0.801 \cdot \sigma_B^{0.712} \quad [\text{unit in MPa}] \quad \text{--- (4)}$$

Where, ${}_c\tau_p$: joint shear strength and σ_B : concrete compressive strength in MPa.

The average value of the ratios [$\tau_p / {}_c\tau_p$] of measured maximum shear stress [τ_p] to calculated strengths [${}_c\tau_p$] by Equation (4) for 50 elastic joint specimens is 1.00 and the standard deviation is 0.102. The measured shear strengths for seven three-dimensional specimens having transverse beams, were higher than the predicted by Equation (4) by about 8% in average.

Relationships between the ratios [$\tau_p / {}_c\tau_p$] and column axial force ratios [η] for 50 elastic specimens are shown in Figure 3. The effect of column axial force ratio on joint shear strength is not significant. Figure 4 shows the variations of the ratios [$\tau_p / {}_c\tau_p$] against the joint shear reinforcement ratio [p_w]. The joint shear reinforcement ratio has a minor effect on shear strength of elastic joints. A similar result was obtained for joint transverse reinforcement strength [$p_w \cdot \sigma_{wy}$]. Use of high yield strength reinforcement for joint hoop was not effective to improve the shear strength. Bond property of beam bars, specimen size and aspect ratio of joint panel did not affect significantly on joint shear strength in this research scope.

SUBASSEMBLAGE DEFORMATION AT BEAM YIELDING

In the database, beam shear force [Q_b] - story drift angle [R] relationships were given by the multi-linear envelope curves as shown in Figure 5, that was characterized by five points: P1 corresponds to the point where the initial stiffness changes, P2 is at beam flexural yield starting, P3 is at maximum load, and P4 and P5 are the points on descending branch after peak.

The story drift angle at beam yielding was analysed using the selected 150 FS and F-type specimens without transverse beams. The selected specimens are the specimens with good bond property of beam bars passing

through beam-column joints. The good bond property was appraised when the bond index $[\mu_B]$ given by Equation (5) satisfied the following criteria.

$$\mu_B = 3.19 \cdot \frac{d_b \cdot \sigma_y}{D_c \cdot \sqrt{\sigma_B}} \leq 12.5 \quad [\text{unit in MPa}] \quad \text{--- (5)}$$

Where, μ_B : bond index, d_b : diameter of longitudinal beam bars through joint and σ_y : yield strength of longitudinal bars.

When the deformation due to the joint shear distortion and the bar slip are ignored, the story drift angle of subassemblage at beam yielding can be calculated by Equation (6), as a sum of the components due to beam and column flexural deformations.

$${}_cR2 = R_b + R_c = \frac{\delta_{b1} + \delta_{b2}}{L_o + D_c} + \frac{\delta_{c1} + \delta_{c2}}{H_o + D_b} \quad \text{--- (6)}$$

$$\delta_b = \frac{Q_{by}}{\alpha_y \cdot K_b}, \quad \delta_c = \frac{Q_c}{\alpha \cdot K_c} \quad \text{--- (7)}$$

$$\alpha_y = (0.043 + 1.64 \cdot n \cdot p_t + 0.043 \cdot \frac{a}{D} + 0.33 \cdot \eta) \cdot (\frac{d}{D})^2 \quad \text{--- (8)}$$

$$\frac{1}{\alpha} = 1 + (\frac{1}{\alpha_y} - 1) \cdot \left\{ \frac{1 - (M_{mc}/M_c)}{1 - (M_{mc}/M_y)} \right\} \quad \text{or} \quad \alpha = 1 \quad \text{when} \quad M_c < M_{mc} \quad \text{--- (9)}$$

Where, R_b : component due to beam deformation, R_c : component due to column deformation, δ_b : beam-end displacement, δ_c : column-end displacement, Q_{by} : beam shear force at beam yielding, Q_c : column shear force at beam yielding, α_y : stiffness deterioration ratio at yielding [empirical equation proposed by SUGANO, which is quoted in *AIJ Standard for Structural Calculation of Reinforced Concrete Structure*], α : column stiffness deterioration ratio at beam yielding, K_c : column elastic stiffness, K_b : beam elastic stiffness, M_{mc} : column flexural crack moment, M_y : column yield moment, M_c : column moment at beam yielding, n : steel to concrete elastic modulus ratio, p_t : tension reinforcement ratio, a/D : shear span to whole depth ratio, η : column axial force ratio and d : effective depth.

Comparison between the measured $[R2]$ and calculated $[_cR2]$ is shown in Figure 6, which indicates that the additional deformation due to slip of beam bars and joint shear distortion cannot be ignored. The additional deformation due to slip of beam bars in joint region $[\delta_s]$ can be simply evaluated by the equations shown in Figure 7. For the specimens that satisfy the Equation (5), the relative slip of beam bars in compression stress is a negligible order when the bars commence yielding in tension at far face of the column. Assuming the bar strain distribution to be linear (zero at compression side and the yield strain at tension side), the slip of tension bars at column face is given by the bar elongation (shaded area of strain distribution in Figure 7). Comparison between measured $[R2]$ and calculated values considering the slip of beam bars $[_cR2^*]$ are shown in Figure 8. Comparing with Figure 6, the improved prediction was obtained. The ratio of the additional deformation due to slips of beam bars $[_cR_{slip}]$ to the measured subassemblage deformation $[R2]$ was 25.7% in average ($_cR_{slip}/R2 = 10.3\% \sim 47.3\%$ with 7.1% in standard deviation). Figure 9 shows the case when the estimation of additional deformation due to joint shear distortion based on the study of KITAYAMA (Table 2) was added to the above calculated value $[_cR2^*]$. In this case, the overall deformation was overestimated. The ratio of the deformation due to joint shear distortion to the measured overall deformation at beam yielding was 28.7% in FS-type, and 17.9% in F-type.

DUCTILITY OF PLASTIC JOINTS FAILED IN JOINT SHEAR

In order to estimate the deformation capacity of plastic joint subassemblage, the characteristic post-peak deformation $[R95]$ was defined, which is the story drift angle when the load decreased to 95% of the maximum load in envelope curves as shown in Figure 5. The ductility ratio $[\mu]$ is given by the ratio, $R95/R2$.

Sixty FS-type specimens without transverse beams were selected for the analysis. The specimens have good bond property of beam bars. The measured ductility ratio $[\mu]$ vs. joint shear to flexural strength ratio $[_c\tau_p/\tau_p]$ relationships is shown in Figure 10. The strength ratio $[_c\tau_p/\tau_p]$ is the ratio of joint shear strength given by Equation (4) $[_c\tau_p]$ to experimental maximum joint shear input $[\tau_p]$ corresponding to beam flexural capacity. There is a tendency that the larger the strength ratio, the higher the ductility ratio. Even for the specimens with $_c\tau_p/\tau_p = 1.0$, a ductility of over two is obtained. Specimens failed in joint shear after load reversals in inelastic

range did not show a rapid decrease in strength in load-deformation curves. The joint strength ratio would be a good index of deformability for plastic joint subassembly.

In order to evaluate the contribution of the joint strength ratio [${}_c\tau_p/\tau_p$] itself, eight specimens were selected which have nearly equal values of other influencing parameters, for which the joint shear reinforcement ratio [p_w] was in from 0.203% to 0.377% and beam bars yield strength [σ_y] was less than 490MPa. Figure 11 shows the relation between the measured ductility ratio [μ] and joint strength ratio [${}_c\tau_p/\tau_p$] for the selected specimens. A strong correlation was obtained and the ductility ratio [μ_0] can be formulated by Equation (10).

$$\mu_0 = 5.36 \cdot \frac{{}_c\tau_p}{\tau_p} - 2.82 \quad \text{--- (10)}$$

Figure 12 shows the relationship between the measured to the calculated ductility ratio by Equation (10) [μ/μ_0] and joint shear reinforcement ratios [p_w] for 33 specimens with less than 490MPa of beam bar yield strength. Ductility ratio tends to be improved with an increase of joint shear reinforcement ratio. The adjustment of Equation (10) to consider the confining effect of joint shear reinforcement can be given by Equation (11).

$${}_c\mu_1 = \mu_0 \cdot \{ 0.437 \cdot (100 \cdot p_w) + 0.873 \} \quad \text{--- (11)}$$

Effect of the yield strength of beam bars was examined using whole 60 specimens. Figure 13 shows the relationship between the measured to calculated ductility ratio by Equation (11) [$\mu/{}_c\mu_1$] and yield strength of beam bars [σ_y]. For the specimens using high strength steel in beam bars, lower ductility ratio was obtained than predicted. Larger yield strain of high strength steel makes the absolute deformation R2 larger, which affects the ductile capacity. Equation (12) was obtained to consider the effect of beam bar yield strength.

$${}_c\mu_2 = {}_c\mu_1 \cdot (1.31 - 0.00081 \cdot \sigma_y) \quad \text{--- (12)}$$

Figure 14 shows the comparison between the measured [μ] and the calculated ductility ratio by Equation (12) [${}_c\mu_2$]. The average of the ratio $\mu/{}_c\mu_2$ was 1.03 and the standard deviation was 0.20. The effects of bond property [μ_B] of beam bars, concrete compressive strength [σ_B] and column axial force ratio [η] were not the decisive factors on the ductility of FS-type specimens in this research scope. However, it should be noted that the poor bond ability induce the poor energy dissipation capacity in load reversals. For practical design purpose, it is required that the measured joint shear stress at beam flexural capacity [τ_p] should be replaced by the calculated value [τ_u]. When τ_u was given by Equation (13) and (14), the average of τ_p/τ_u was 1.12 for the specimens of this database. Accordingly, it could be done by replacing τ_p by $1.12 \cdot \tau_u$ in Equation (10), (11) and (12).

$$\tau_u = \frac{(M_{bu1} / j_1) + (M_{bu2} / j_2) - Q_c}{b_j \cdot D_j} \quad \text{--- (13)}$$

$$M_{bu} = \frac{7}{8} \cdot a_t \cdot \sigma_y \cdot d \quad \text{--- (14)}$$

Where, M_{bu} : ultimate flexural moment of beam and a_t : total area of tension reinforcement.

DUCTILITY OF PLASTIC JOINT FAILED IN BEAM FLEXURE

For the F-type specimens, the ultimate deformability is governed by the plastic hinge rotational capacity at beam ends. Figure 15 shows the correlations between the measured ductility ratios [μ] and bond index [μ_B] for selected 26 F-type regular specimens without transverse beams. Smaller ductility ratio was measured for specimens with larger bond index. Poor bond property in joint region makes internal concrete compressive force large at column face, which result in the early concrete crushing under load reversals in plastic range.

PREDICTION OF FINAL FAILURE MODE

Figure 16 shows the relationships between the shear to flexural strength ratios [${}_c\tau_p/\tau_p$] and calculated ductility ratios [${}_c\mu_2$] by Equation (12) for F and FS-type specimens with good bond properties [$\mu_B \leq 12.5$]. When the ratio

$c\tau_p/\tau_p$ is larger than 1.6, joint shear failure does not occur. When the ratio $c\tau_p/\tau_p$ is larger than 1.3, the subassemblage has a deformation capacity with ductility ratio of more than 4.0.

CONCLUSIONS

In order to estimate the earthquake resistant capacities of interior R/C beam-column joint subassemblage, the database study was conducted. Following findings were obtained:

For elastic joints, (1) Joint shear strength was greatly influenced by concrete compressive strength [σ_B]. However, column axial force ratio and joint shear reinforcement ratio were not major influencing factors. (2) Joint shear strength equation can be developed by regression analysis, which is proportional to $\sigma_B^{0.712}$ in the range of $18\text{MPa} \leq \sigma_B \leq 117\text{MPa}$.

For inelastic joints, (1) The additional deformation due to slips of beam bars at the joint region cannot be ignored in the evaluation of the overall subassemblage deformation at beam yielding. (2) Specimens failed in joint shear after load reversals in inelastic range did not show a rapid decrease of the strength in load-deformation curves. (3) The ductility ratio of subassemblage governed by joint shear failure could be formulated as a function of the joint strength ratio [$c\tau_p/\tau_p$: ratio of joint shear strength to joint shear input corresponding to beam flexural capacity], joint shear reinforcement ratio [p_w] and the yield strength of beam bars [σ_y]. (4) The proposed equations provide a good agreement between calculated and measured ductility of available 60 specimens, and it can predict the final failure modes of specimens with an excellent accuracy.

REFERENCES

- Architectural Institute of Japan 1988. Design Guideline for Earthquake Resistant Reinforced Concrete Building Based on Ultimate Strength Concept (in Japanese).
- Architectural Institute of Japan 1991. Standard for Structural Calculation of Reinforced Concrete Structure (in Japanese)
- Architectural Institute of Japan 1997. Design Guideline for Earthquake Resistant Reinforced Concrete Building Based on Inelastic Displacement Concept (Draft) (in Japanese)
- K. Kitayama 1992. Restoring Force Characteristics in Reinforced Concrete Beam-Column Joints (in Japanese). Proceedings of the Japan Concrete Institute, Vol.14-2, 431-436

Table 1 Range of experimental parameters

Element data		F-type 129 specimens	FS-type 144 specimens	S-type 59 specimens
Column section [$b_c \times D_c$]	(mm)	220 x 220 ~ 850 x 850	220 x 220 ~ 660 x 660	150 x 150 ~ 460 x 500
Beam section [$b_b \times D_b$]	(mm)	160 x 220 ~ 520 x 750	150 x 250 ~ 600 x 600	150 x 150 ~ 400 x 630
Aspect ratio of joint panel [D_c / D_b]		0.83 ~ 2.00	0.75 ~ 1.19	0.57 ~ 1.13
Concrete compressive strength [σ_B]	(MPa)	18.7 ~ 92.6	19.3 ~ 117	20.6 ~ 107
Yield strength of beam bars [σ_y]	(MPa)	283 ~ 858	288 ~ 913	345 ~ 1069
Yield strength of joint shear reinforcement [σ_w]	(MPa)	300 ~ 1451	235 ~ 1456	291 ~ 1392
Joint shear reinforcement ratio [p_w]*	(%)	0.00 ~ 2.10	0.00 ~ 2.44	0.00 ~ 1.72
Joint transverse reinforcing strength [$p_w \cdot \sigma_w$]	(MPa)	0 ~ 13.0	0 ~ 9.35	0 ~ 6.52
Column axial force ratio [η]		0.000 ~ 0.480	0.000 ~ 0.440	0.000 ~ 0.485

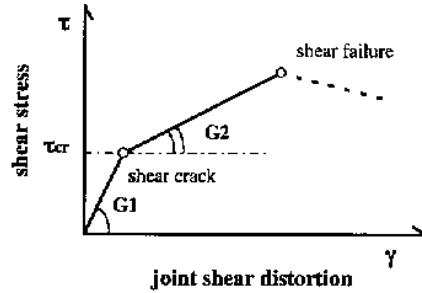
* Joint shear reinforcement ratio : $p_w = a_w / (b_c \cdot j)$

where, a_w : total area of joint shear reinforcement between top and bottom beam bars, b_c : column width and j : internal lever arm in beam section.

Table 2 Estimation of the joint shear distortion based on the study of KITAYAMA

$$\tau_{cr} = \sqrt{\sigma_o \cdot f_t + f_t^2}, \quad G_1 = \frac{E_c}{2 \cdot (1 + \nu)}, \quad G_2 = 16260 \cdot K_0 \cdot K_1 \cdot K_2 \cdot K_3 \quad (\text{unit in } \text{kgf/cm}^2)$$

$$\begin{aligned} \nu &= 4 \times 10^{-5} \cdot \sigma_B + 0.169 \\ K_0 &= 0.143 \cdot \sigma_B^{0.327} & (\sigma_B < 962 \text{kgf/cm}^2) \\ &= 1.35 & (\sigma_B \geq 962 \text{kgf/cm}^2) \\ K_1 &= 1.00 & (p_w < 0.27\%) \\ &= 1.184 \cdot p_w^2 - 0.411 \cdot p_w + 1.025 & (0.27\% \leq p_w < 1.27\%) \\ &= 2.41 & (1.27\% \leq p_w) \\ K_2 &= 0.261 \cdot p_{ci} + 0.778 & (p_{ci} < 0.85\%) \\ &= 1.00 & (p_{ci} \geq 0.85\%) \\ K_3 &= -2.83 \times 10^{-3} \cdot \sigma_o + 1.057 & (\sigma_o < 80 \text{kgf/cm}^2) \\ &= 0.83 & (\sigma_o \geq 80 \text{kgf/cm}^2) \end{aligned}$$



Where, τ_{cr} : shear stress at shear crack of joint region, G_1 : initial stiffness, G_2 : the second stiffness, σ_o : column axial stress, f_t : concrete split tensile strength, ν : Poisson's ratio, E_c : concrete elastic modulus and p_{ci} : vertical joint shear reinforcement ratio (intermediate column bars)

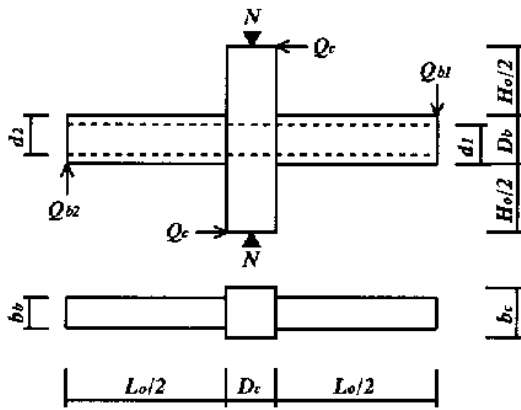


Fig. 1 Shape of specimens and loading conditions

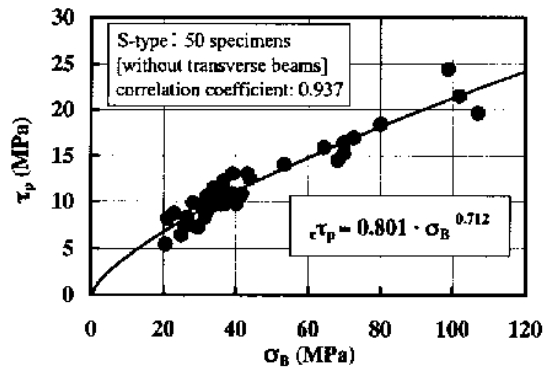


Fig. 2 Joint shear strength [τ_p] - concrete compressive strength [σ_B] relationship

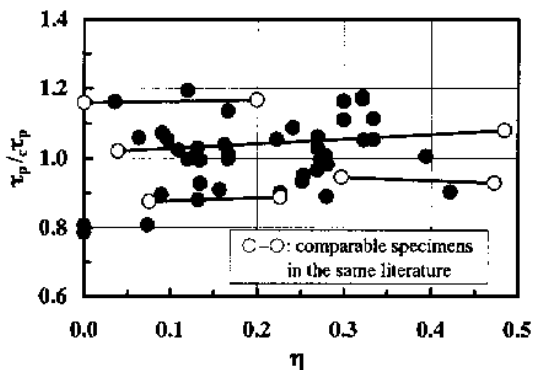


Fig. 3 Effect of column axial force ratio [η] on the ratios of measured to calculated joint shear strength by Eq.(4) [τ_p / τ_{cr}]

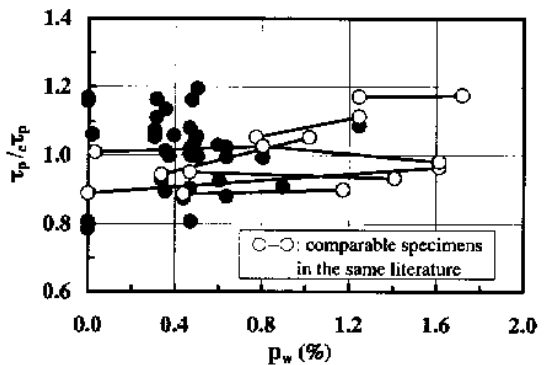
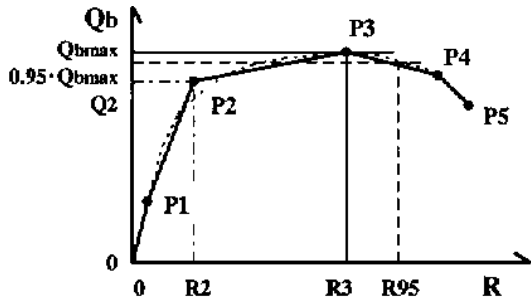


Fig. 4 Effect of joint shear reinforcement ratio [p_w] on the ratios of measured to calculated joint shear strength by Eq.(4) [τ_p / τ_{cr}]



P1: correspond to the point where the initial stiffness changes
 P2: at beam flexural yield starting
 P3: at maximum load
 P4 and P5: the points on descending branch after peak

Fig. 5 Characteristic points of beam shear force $[Q_b]$ - story drift angle $[R]$ curve

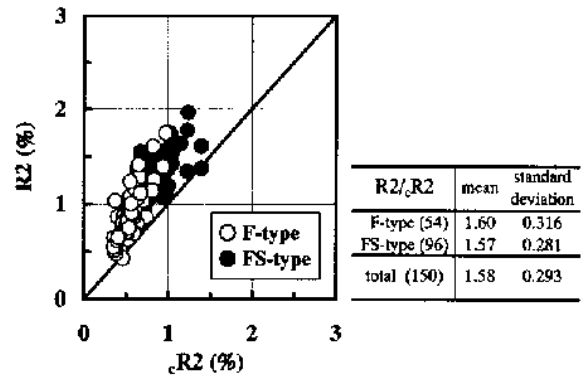
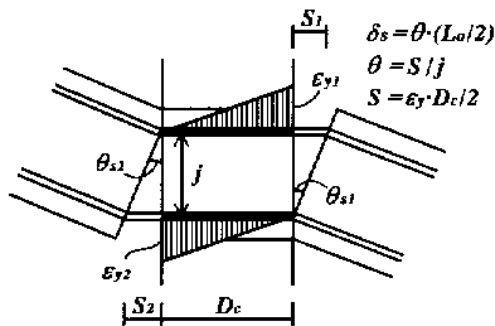


Fig. 6 Comparison between measured $[R2]$ and calculated drift angle $[cR2]$ at beam yielding (Additional deformation due to slips of beam bars and joint shear distortion were ignored.)



where, δ_s , θ : additional deformation and rotation due to slips of beam bars, S : slips of beam bars and ϵ_y : yield strain of beam bars.

Fig. 7 Calculation of the additional deformation due to slips of beam bars at joint region

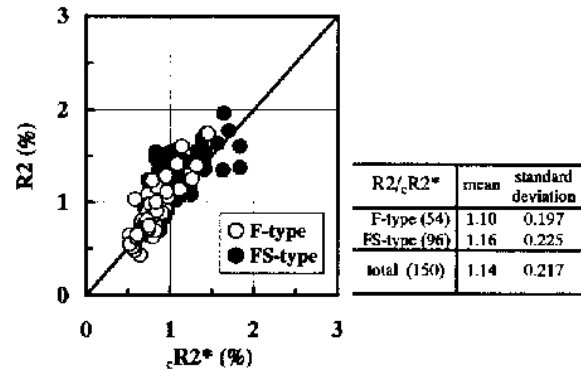


Fig. 8 Comparison between measured $[R2]$ and calculated deformation $[cR2^*]$ at beam yielding (Additional deformation due to slips of beam bars is considered.)

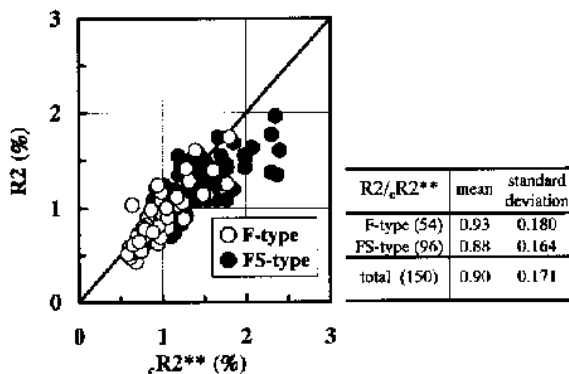


Fig. 9 Comparison between measured $[R2]$ and calculated deformation $[cR2^{**}]$ at beam yielding (Additional deformation due to slips of beam bars and joint shear distortion are considered.)

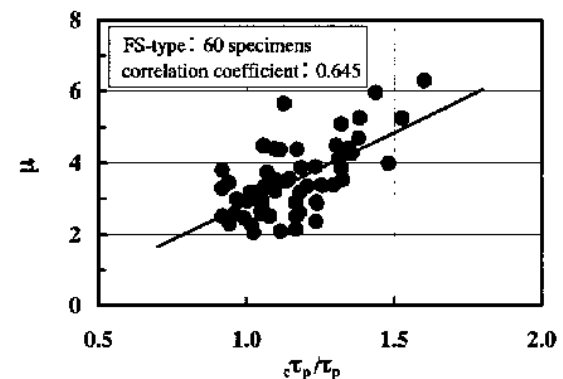


Fig.10 Measured ductility ratio $[\mu]$ vs. joint shear to flexural strength ratio $[c\tau_p/\tau_p]$ relationships for available 60 FS-type specimens

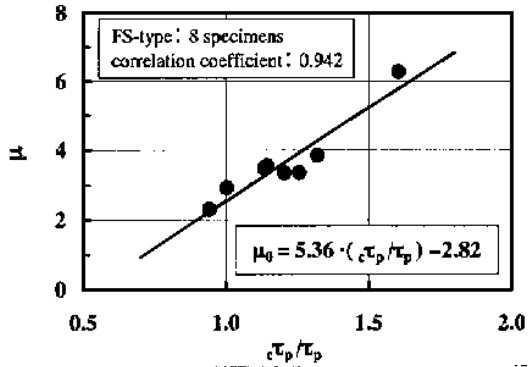


Fig.11 Measured ductility ratio $[\mu]$ vs. joint shear to flexural strength ratio $[c\tau_p/\tau_p]$ relationships for selected comparable specimens

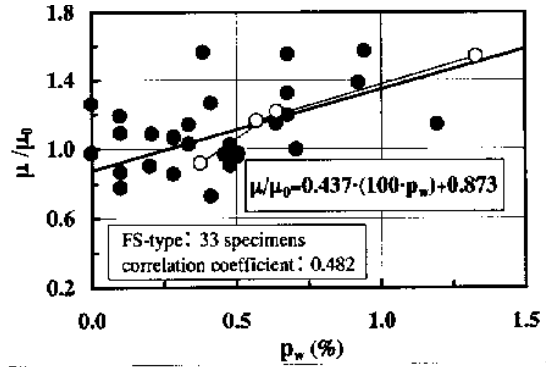


Fig.12 Effect of joint shear reinforcement ratio $[\rho_w]$ on the ratios of measured to calculated ductility ratio by Eq.(10) $[\mu/\mu_0]$

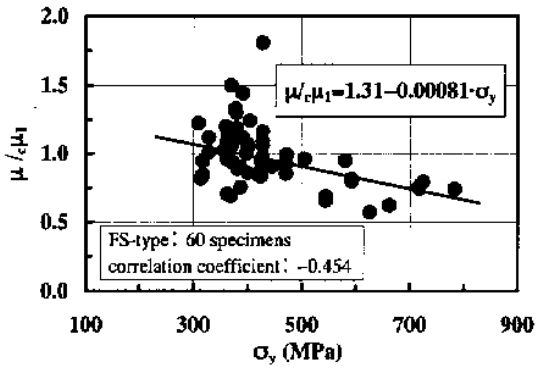


Fig.13 Effect of yield strength of beam bars $[\sigma_y]$ on the ratios of measured to calculated ductility ratio by Eq.(11) $[\mu_c/\mu_c]$

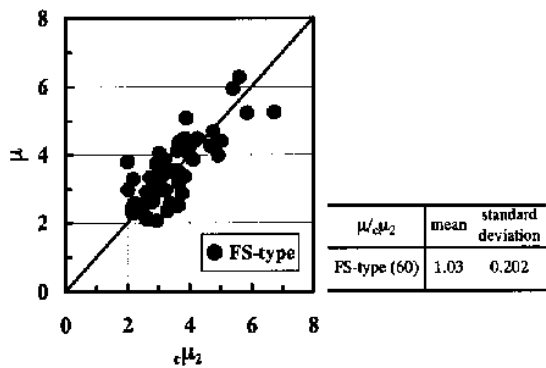


Fig.14 Comparison between measured $[\mu]$ and calculated ductility ratio by Eq.(12) $[c\mu_2]$

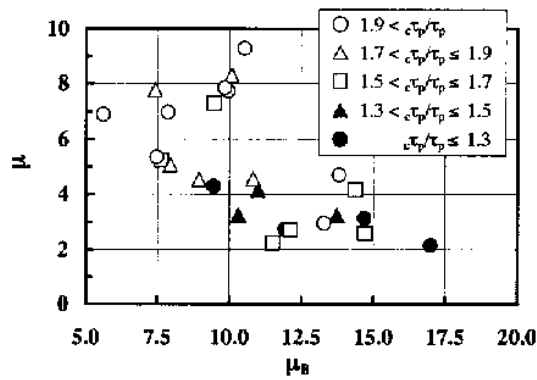


Fig.15 Measured ductility ratio $[\mu]$ vs. bond index $[\mu_B]$ relationships

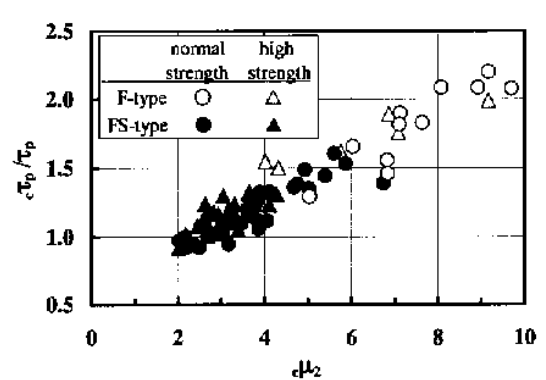


Fig.16 Classification of failure modes and ductility prediction by joint shear to flexural strength ratio $[c\tau_p/\tau_p]$